ELSEVIER

Surface Science 344 (1995) 149–158

surface science

MCTDH study of CH_4 dissociation on Ni(111)

A.P.J. Jansen *, H. Burghgraef

Laboratory of Inorganic Chemistry and Catalysis, Eindhoven University of Technology, P.O. Box 513, 5600 MB Eindhoven, The Netherlands

Received 4 May 1995; accepted for publication 3 August 1995

Abstract

We present results of quantum simulations using the multi-configuration time-dependent Hartree method for the dissociation of CH_4 on Ni(111) with a potential-energy surface based on density-function calculations. As varied coordinates we include the distance of the methane molecule to the surface, a C–H distance, and the orientation of the CH_4. Taking into account the latter coordinate decreases the dissociation probability. For the range of translational energies we studied, the dissociation occurs via tunneling.

Keywords: Alkanes; Computer simulations; Low index single crystal surfaces; Surface chemical reaction

1. Introduction

The dissociation of CH_4 on transition metals is very interesting for a number of reasons. In steam reforming to produce H_2 the dissociation is the rate limiting step [1]. More general, as methane is the simplest of all alkanes, its dissociation can be viewed as prototypical for C–H activation in catalysis. It is with this in mind that we started some years ago with density-functional theory (DFT) calculations of the dissociation on nickel. Another reason for our interest are a number of molecular beam experiments in which the dissociation probability was measured as a function of translational energy [2–8]. These experiments have contributed much to our understanding of the mechanism of the dissociation. Also some information has been obtained on the role the internal degrees of freedom play. However, our knowledge is still negligible compared to what we know about a well-studied reaction as H_2 dissociation on copper [9].

In a number of previous studies we have calculated the reaction rate constant of CH_4 dissociation on Ni(111) using DFT and transition-state theory (TST) [10–14]. These studies have shown that there is a late activation barrier. We calculated various heights of this barrier, the most accurate one, in our view, being 121 $kJ \cdot mol^{-1}$. The barrier height could not be obtained reliably either from the experiment, as very different numerical values were obtained depending on the assumed reaction mechanism; precursor or not, tunneling or not. Although our calculations gave results consistent with experiment, they were unsatisfactory, because they yielded only thermally averaged dissociation probabilities, and could therefore not be compared directly with the more detailed molecular beam experiments.

Neither did our calculations yield much informa-

* Corresponding author. Address in 1995: Laboratory of Physics, Helsinki University of Technology, 02150 Espoo, Finland; E-mail: tgtatj@chem.tue.nl.

SSDI 0039-6028(95)000845-4

tion on the role of the internal vibrations. It was observed experimentally that vibrationally hot CH_4 dissociates more readily than cold CH_4, with the energy in the internal vibrations being about as effective as the translational energy in inducing dissociation. However, a more detailed assessment of the importance of the internal vibrations could not be made, because of the large number of internal vibrations. For these reasons we decided to do quantum simulations on the potential-energy surface (PES) that we obtained with our DFT calculations, thus obtaining a better assessment of the quality of these latter calculations.

The quantum simulations have been done using the multi-configuration time-dependent Hartree (MCTDH) method [15,16]. This is a rather new method which has been developed to deal with a large number of degrees of freedom and with large grids. The method has been successfully applied to gas phase reactions (photodissociation of NOCl [15], NO_2 [17], CH_3I [18,19] and ICN [20], vibrational predissociation of Cl_2Ne [21] and the hydrogen exchange reaction $H_2 + H \rightarrow H + H_2$ [22]), but also to reactions at surfaces (photodissociation CH_3I on MgO [23,24], H_2 dissociation on surfaces [16] and H_2 scattering from LiF(001) [25]). The most advanced work has been done on three coupled 5D potential-energy surfaces [18,19]. Much of the work has, however, been directed at testing the method, by choosing models for which other methods were used as well for comparison. This paper presents one of the first real applications of MCTDH to a surface reaction.

2. Computational details

2.1. The potential-energy surface

Some time ago we did DFT calculations on the dissociation of CH_4 on Ni(111) using cluster models [10–14]. We have based the PES on the results of these calculations. As various clusters were used to model the Ni(111) surface, and the results of these calculations were not all the same, we have first identified common characteristics. These consisted of the structure of the transition state for the dissociation, the vibrational frequencies of the adsorbed products CH_3 and H, and, of course, the vibrational frequencies of the CH_4 in the gas phase. Two important parameters that we have not taken from the DFT calculations are the reaction energy and the height of the barrier. The reaction was endothermic for all DFT calculations, whereas experimentally it is found to be slightly exothermic [5]. We have assumed the reaction to be thermodynamically neutral. Many clusters we used gave more or less the same barrier of about 200 $kJ \cdot mol^{-1}$, which is about a factor two higher than the highest experimental estimates [5,26]. Only a Ni_{13} cluster gave a reasonable barrier height of 121 $kJ \cdot mol^{-1}$. We have decided to fit the barrier height to the experimental dissociation probability at the translational energy of 64 $kJ \cdot mol^{-1}$. This is roughly in the middle of the range of translational energies in the experiment [5].

The DFT calculations have optimised four coordinates describing the dissociating CH_4, and vibrational frequencies have been determined explicitly for six coordinates [13]. Our quantum simulations have only been done for three coordinates. Three reasons can be given for this. First, at this moment it is not possible to do a fully quantum simulation with six coordinates for CH_4 dissociation on Ni(111). Second, the DFT calculations provided us with information of the PES only for three small regions in configuration space for CH_4; namely, far from the surface, around the top of the barrier of the PES, and for CH_3 and H on the surface. As the quantum simulations need a complete PES, we had to interpolate, which proved to be taxing even for just three coordinates. Third, it is not clear how important the various coordinates are. We have included the distance of CH_4 to the surface, the distance between the H atom that splits off and the CH_3 that is formed, and the orientation of the CH_3/CH_4. The first two coordinates are evident. The reason for including the third coordinate is that the DFT calculations showed that the orientation of the CH_3 that is formed at the transition state always corresponds with a tilting vibration with a very low frequency (only a few wavenumbers), whereas on the Ni_7 cluster the CH_3 orientation even dominates the reaction coordinate. (On all other clusters the

CH_3–H stretch corresponds to the reaction coordinate.) We have also done a few simulations with a fourth coordinate representing a lattice mode, very much as has been done in the simulations of CH_4 dissociation on Pt(111) [27–29]. In agreement with experimental findings, that showed no [5] or only a small [26] effect of the substrate temperature for Ni(111), we found that these 4D simulations gave similar results as the 3D simulations, and we did not continue with them. We like to note that in this decision computer time was only a minor issue, as for this system the 4D MCTDH simulations took only twice as long as the 3D simulations. No results of the 4D simulations will be presented.

The PES consists of two parts,

$$V(Z, s, \tau) = V_{\text{stretch}}(Z, s) + V_{\text{tilt}}(s, \tau), \tag{1}$$

where Z is the distance between the centre-of-mass of CH_4 and the plane through the nuclei of the atoms in the first layer of the Ni(111) surface, s is the distance between the H atom that splits off and the centre-of-mass of the CH_3 that is formed, and τ is the angle between the threefold axis of this CH_3 and the surface normal. The second term is given by

$$V_{\text{tilt}}(s, \tau) = AS\left(\frac{s - s_1}{s_2 - s_1}\right)(\cos\tau - 1), \tag{2}$$

with $A = -308\ \text{kJ}\cdot\text{mol}^{-1}$, and S is a switch function,

$$S(x) = \begin{cases} 0, & \text{if } x \leqslant 0, \\ 1, & \text{if } x \geqslant 1, \\ 10x^3 - 15x^4 + 6x^5, & \text{if } 0 \leqslant x \leqslant 1, \end{cases} \tag{3}$$

which is continuous and has continuous first and second derivatives everywhere. The constants $s_1 = 0.169$ nm and $s_2 = 0.287$ nm correspond to the top of the barrier and the CH_3–H distance where the dissociation is complete, respectively. These values, and also the value of A, have been obtained directly from the DFT calculations. Note that there is no τ-dependence up to the top of the barrier. This is reasonable for the CH_4 prior to dissociation as CH_4 is spherical to a good approximation. But also at the top of the barrier the DFT calculations show only a very weak τ-dependence.

The first term in Eq. (1) is given by a generalisation of a LEPS form [30],

$$V_{\text{stretch}}(Z, s) = U_Z(Z) + U_s(s) - \sqrt{Q_Z^2(Z) + Q_s^2(s) - Q_Z(Z)Q_s(s)}, \tag{4}$$

with

$$U_Z(Z) = \epsilon_Z(\alpha_Z\, e^{-2\gamma_Z(Z - Z_0)} + \beta_Z\, e^{-\gamma_Z(Z - Z_0)}), \tag{5}$$

$$Q_Z(Z) = \epsilon_Z[(1 - \alpha_Z)\, e^{-2\gamma_Z(Z - Z_0)} - (2 + \beta_Z)\, e^{-\gamma_Z(Z - Z_0)}], \tag{6}$$

and similar expressions for U_s and Q_s. In the asymptotic limits $Z \to \infty$ and $s \to \infty$ the potential V_{stretch} becomes the Morse potential $U_s + Q_s$ and $U_Z + Q_Z$, respectively. The parameters are given by $\epsilon_Z = \epsilon_s = 480\ \text{kJ}\cdot\text{mol}^{-1}$, $Z_0 = 0.206$ nm, $s_0 = 0.115$ nm, $\gamma_Z = 11.0\ \text{nm}^{-1}$, $\gamma_s = 17.4\ \text{nm}^{-1}$, $\alpha_Z = 0.6596$, $\alpha_s = 1.3867$, $\beta_Z = -0.6999$ and $\beta_s = -0.2281$. The parameters ϵ_s and ϵ_Z are obtained, using DFT, from the dissociation energy for CH_4 in the gas phase and the assumption that the reaction on Ni(111) is thermodynamically neutral. The parameters s_0 and Z_0 are obtained from the optimised geometries we determined with DFT. The parameter γ_Z is derived by fitting to the vibrational frequencies of the products as determined by the DFT calculations. Analogously, the parameter γ_s is obtained from the CH_3–H stretch vibration in the gas phase. The other parameters are chosen to give a top of the barrier of the PES at $Z = 0.222$ nm and $s = 0.169$ nm, and a barrier height of $93.2\ \text{kJ}\cdot\text{mol}^{-1}$. The position is once again determined by DFT calculations, but we choose the height to obtain a dissociation probability equal to the experimental one at a translational energy of CH_4 of $64\ \text{kJ}\cdot\text{mol}^{-1}$. In fact, the number of parameters is overcomplete to determine just the barrier. The remaining freedom had to be used to avoid a deep physisorption minimum at low Z and low s. Fig. 1 shows a plot of V_{stretch}. In agreement with the experimental observations of increased dissociation probability by vibrational excitation we find a very late barrier.

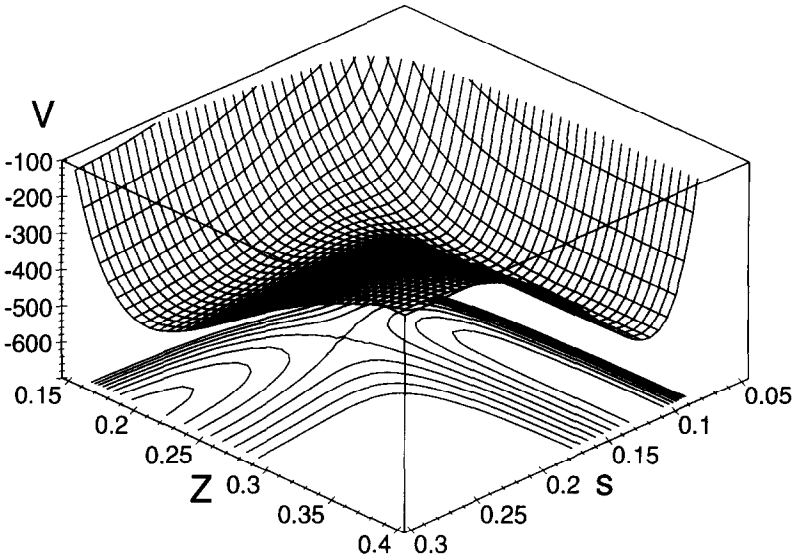

Fig. 1. The potential-energy surface in the $\tau = 0$ plane. Contours are drawn at intervals of 23.3 kJ · mol^{-1}. The coordinates are given in nm, and the energies on the left in kJ · mol^{-1}.

2.2. Initial and final states

The initial states in the simulation are given by

$$\Psi(Z, s, \tau) = \psi^{(\mathrm{tr})}(Z)\psi^{(\mathrm{stretch})}_{v_s}(s)\psi^{(\mathrm{rot})}_{m_\tau}(\tau). \tag{7}$$

In this expression $\psi^{(\mathrm{tr})}$ represents the initial translational part. It is a Gaussian wavepacket,

$$\psi^{\mathrm{tr}}(Z) = (2\pi\sigma^2)^{-1/4} \exp\left(-\frac{(Z - Z_0)^2}{4\sigma^2} + \mathrm{i}P_Z Z \right), \tag{8}$$

where Z_0 is the initial position of the wavepacket (we used $Z_0 = 0.582$ nm), σ is the width, which was chosen large to have a small spread in momentum and energy (we used $\sigma = 0.0468$ nm), and P_Z is the initial momentum. The s-dependence of Ψ is given by $\psi^{(\mathrm{stretch})}_{v_s}$, which is an eigenstate of the Hamiltonian for the CH_3–H stretch in the gas phase. The potential in this Hamiltonian is given by $U_s + Q_s$. The index labels the various eigenstates; $v_s = 0$ for the ground state, and $v_s = 1, 2, 3, \ldots$ for the excited states. The τ-dependence is given by

$$\psi^{(\mathrm{rot})}_{m_\tau}(\tau) = \begin{cases} (1/\sqrt{\pi})\cos(m\tau), & \text{if } m \geqslant 0, \\ 1/\sqrt{2\pi}, & \text{if } m = 0, \\ (1/\sqrt{\pi})\sin(|m|\tau), & \text{if } m < 0. \end{cases} \tag{9}$$

As there is no τ-dependence for $Z \to \infty$ in the PES, it would be more natural to choose $\exp(im\tau)$. But as $\exp(im\tau)$ and $\exp(-im\tau)$ are degenerate, the definition above is also valid. It has the advantage that it is adapted to the mirror symmetry in τ of the PES.

The states $\psi^{(\mathrm{stretch})}_{v_s}$ and $\psi^{(\mathrm{rot})}_{m_\tau}$ are eigenstates for $Z \to \infty$, and we will be interested in the population of these eigenstates for the scattered part of the wavefunction. The dissociated part of the wavefunction we will project on $\psi^{(\mathrm{norm})}_{v_Z}(Z)$ and on $\psi^{(\mathrm{tilt})}_{v_\tau}(\tau)$. Here $\psi^{(\mathrm{norm})}_{v_Z}$ is an eigenstate of the Hamiltonian for the vibration of the dissociated CH_4 as a whole normal to the surface (potential $U_Z + Q_Z$), and $\psi^{(\mathrm{tilt})}_{v_\tau}$ is an eigenstate of the Hamiltonian for the CH_3 tilt motion (potential $A(\cos\tau - 1)$). We have $v_Z, v_\tau = 0, 1, 2, \ldots$, where higher indices mean higher excitation levels.

2.3. The multi-configuration time-dependent Hartree method

As this method has been described extensively elsewhere we will give here only an outline. We have used MCTDH with equations of motion for the natural single-particle functions [16]. The total

wavefunction Ψ is written as

$$\Psi(q_1,\ldots,q_D;t)=\sum_{n_1\ldots n_D} c_{n_1\ldots n_D}(t) \times \psi^{(1)}_{n_1}(q_1;t)\cdots\psi^{(D)}_{n_D}(q_D;t), \quad (10)$$

where $\psi^{(j)}_{n_j}$ are the natural single-particle functions, which are defined as a eigenstate of the reduced density operator

$$\rho_j(q_j,q_j')=\int \mathrm{d}q_1\cdots\mathrm{d}q_{j-1}\mathrm{d}q_{j+1}\cdots\mathrm{d}q_D \times\Psi(q_1,\ldots,q_{j-1},q_j,q_{j+1},\ldots,q_D) \times\Psi^*(q_1,\ldots,q_{j-1},q_j',q_{j+1},\ldots,q_D). \quad (11)$$

The equations of motions for the natural single-particle functions can be obtained by differentiation of the eigenvalue equation. This gives us

$$\mathrm{i}\hbar\frac{\partial}{\partial t}\psi^{(j)}_{n_j}=h_j\psi^{(j)}_{n_j}+\sum_{m_j}B^{(j)}_{n_jm_j}\psi^{(j)}_{m_j} +\frac{\langle\tilde\psi^{(j)}_{n_j}|V|\Psi\rangle}{\langle\tilde\psi^{(j)}_{n_j}|\tilde\psi^{(j)}_{n_j}\rangle}-\sum_{m_j}\frac{\langle\psi^{(j)}_{m_j}\tilde\psi^{(j)}_{n_j}|V|\Psi\rangle}{\langle\tilde\psi^{(j)}_{n_j}|\tilde\psi^{(j)}_{n_j}\rangle}\psi^{(j)}_{m_j}, \quad (12)$$

where

$$B^{(j)}_{n_jm_j}=\frac{\langle\psi^{(j)}_{m_j}\tilde\psi^{(j)}_{n_j}|V|\Psi\rangle-\langle\Psi|V|\psi^{(j)}_{n_j}\tilde\psi^{(j)}_{m_j}\rangle}{\langle\tilde\psi^{(j)}_{n_j}|\tilde\psi^{(j)}_{n_j}\rangle-\langle\tilde\psi^{(j)}_{m_j}|\tilde\psi^{(j)}_{m_j}\rangle} \quad (13)$$

and

$$\tilde\psi^{(j)}_{n_j}=\sum_{n_1\ldots n_{j-1}}\sum_{n_{j+1}\ldots n_D}c_{n_1\ldots n_D} \times\psi^{(1)}_{n_1}\cdots\psi^{(j-1)}_{n_{j-1}}\psi^{(j+1)}_{n_{j+1}}\cdots\psi^{(D)}_{n_D}. \quad (14)$$

The Hamiltonian H is given by

$$H=\sum_{j=1}^{D}h_j+V. \quad (15)$$

Differentiation of

$$c_{n_1\ldots n_D}=\langle\psi^{(1)}_{n_1}\cdots\psi^{(D)}_{n_D}|\Psi\rangle \quad (16)$$

gives us

$$\mathrm{i}\hbar\frac{\mathrm{d}}{\mathrm{d}t}c_{n_1\ldots n_D}=\langle\psi^{(1)}_{n_1}\cdots\psi^{(D)}_{n_D}|V|\Psi\rangle -\sum_{j=1}^{D}c_{n_1\ldots n_{j-1}m_jn_{j+1}\ldots n_D}B^{(j)}_{m_jn_j}. \quad (17)$$

Eqs. (12) and (17) are to be solved numerically. More general equations of motion can be derived starting from a time-dependent variational principle [15]. It has explicitly been shown that Eqs. (12) and (17) are recovered by imposing appropriate restrictions [31,32]. We find that these equations are somewhat more convenient to analyse results than the more general equations of motion. In particular, it is easy to determine the convergence of the simulations with respect to the number of terms (configurations) in Eq. (10). However, other equations of motion may be numerically more advantageous by allowing a larger step size in the numerical integration. This is very much still an open question. We have used the variable-order variable-step Adams method as implemented in routine D02CBF of the NAG library for the numerical integration [33,34]. The length of each simulation was 360 fs.

The grid that we have used spans the region $0.132\leqslant Z\leqslant 0.807$ nm, $0.053\leqslant s\leqslant 1.405$ nm, and $-\pi\leqslant\tau<\pi$ in configuration space. There are 256 grid points in Z, 512 in s, and 64 in τ. The large range in s was necessary as the H atom that splits off moves very fast, and very far, over the surface. The grid has also to be dense, because of the high mass of CH_4. Such a large grid presents no problem at all for MCTDH. Our system is very close to the limiting case where the computer time used by MCTDH scales linearly with the number of grid points *for one coordinate*. The other limiting case is where MCTDH scales exponentially with the number of natural single-particle functions for one coordinate [15]. The number of configurations we used was $7\times7\times4$, which means seven natural single-particle functions for Z, seven for s, and four for τ. Calculations with more natural single-particle functions showed only a negligible difference for the range of translational energy that we looked at.

3. Results and discussion

Fig. 2 shows the dissociation probability for a ground state CH_4 molecule as a function of translational energy. We see that it scales approximately exponentially with the translational energy, except for large probabilities, which is in agreement with

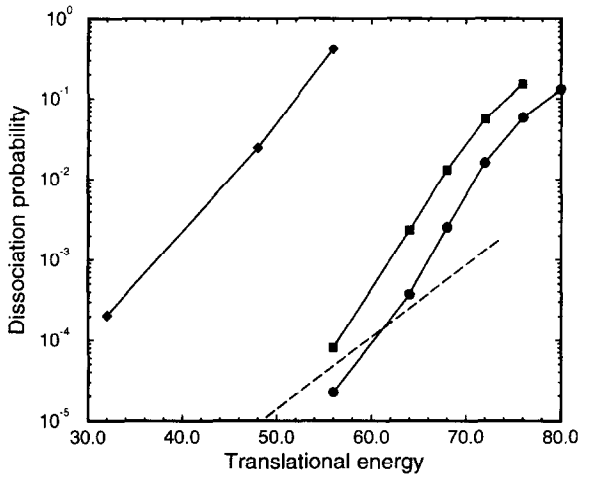

Fig. 2. Dissociation probabilities as a function of translational energy (in $kJ \cdot mol^{-1}$) for CH_4 initially in the ground state (squares: 2D; circles: 3D), for CH_4 with singly excited CH_3–H stretch (diamonds), and from the experiment (dashed line). The symbols are simulation results, and the solid lines are guides for the eye.

the experiment [5]. This has been interpreted as an indication that the dissociation occurs via tunneling. We will show below that this is indeed correct. We have fitted the barrier height of the PES to the experiment, but we see that the curve of the simulation is much steeper than the experimental one. This implies that the barrier of the PES that we used is too wide and too low. To obtain some idea of the error in our barrier height and width we estimate an improved height and width of the barrier as follows. The experimental results have been interpreted using [35]

$$P_{\mathrm{diss}} = \exp\left(-\pi W \sqrt{\frac{\mu}{\hbar^2 E_{\mathrm{bar}}}} (E_{\mathrm{bar}} - E_{\mathrm{T}}) \right) \qquad (18)$$

for the dissociation probability P_{diss} as a function of the translational energy E_{T}, the height E_{bar}, the width W of the barrier, and the mass μ corresponding to the reaction coordinate. The barrier height of our PES is $E_{\mathrm{bar}} = 93.2\ kJ \cdot mol^{-1}$, which gives us for the width $W = 0.0546$ nm using $P_{\mathrm{diss}} = 3.66 \times 10^{-4}$ at $E_{\mathrm{T}} = 64\ kJ \cdot mol^{-1}$, and using for μ the reduced mass of the H atom that splits off. Using $E_{\mathrm{bar}} = 108\ kJ \cdot mol^{-1}$ and $W = 0.04$ nm gives the same dissociation probability at $E_{\mathrm{T}} = 64\ kJ \cdot mol^{-1}$, but these latter values fit the experimental dissociation probability also for other energies [5]. We see that the barrier should be higher and narrower. Eq. (18) is really only valid for a particular 1D model of tunneling. If we use all our simulation results and fit them with Eq. (18) we find $E_{\mathrm{bar}} = 84.1\ kJ \cdot mol^{-1}$ and $W = 0.0725$ nm. The difference with the real barrier height is a consequence of the fact that our simulations are 3D and not 1D. One consequence of this is that zero-point vibrations perpendicular to the reaction coordinate changes the effective barrier height (see below). Also the twelve degrees of freedom of CH_4 we do not include in our simulations will have an effect on the effective barrier height. There is a whole range of experimental values for the barrier height, 33.0 [8], 52.7 [36], 108.7 [5] and about $130\ kJ \cdot mol^{-1}$ [26], but there is a fair agreement between values based on a dynamical interpretation of experimental results [5,26] and our value of $93.2\ kJ \cdot mol^{-1}$, and also the value of $121\ kJ \cdot mol^{-1}$ we calculated with DFT.

The tunneling mechanism has recently been questioned in the case of H_2 dissociation on copper. Instead, the dissociation probability has been explained classically by the hole model [37]. This model uses a distribution of barrier heights. At higher energy the hole in configuration space through which the system can pass from reactant to product is bigger than at low energy. It has been remarked, however, that it would be unlikely that a distribution of barriers would produce the exponential scaling [5]. It is absolutely clear that in the simulations we are seeing tunneling, as the incoming methane molecule simply does not have enough energy (translational and $15.9\ kJ \cdot mol^{-1}$ zero-point vibrational energy) to get over the barrier. This does not mean that tunneling is important for the thermally averaged dissociation probability. The contribution from high energies has a small Boltzmann factor, and at low energies there is a smll dissociation probability. It is still an open question whether the largest contributions come from energies below or above the activation energy. The results from Beebe et al. [36] seem to suggest the former, whereas our TST results suggest the latter [11–14].

Fig. 2 also shows the effect that including the

rotation of methane has. We see that the dissociation probability in the 2D simulations, without the coordinate τ, is about a factor of five larger than in the 3D simulations. One way to understand this is by using a model with 1D effective potentials [38,39]. We first define a reaction path as a steepest-descent path from the top of the barrier. We do this in the configuration space of mass-weighted coordinates as otherwise the reaction path cannot be defined unambiguously [40]. Next we define an effective potential as a function of the reaction coordinate as the sum of the value of the PES on the reaction path plus an eigenvalue corresponding to the vibrations perpendicular to the reaction path. The results are shown in Fig. 3. In the entrance channel there is no difference between the 2D and the 3D case for $m_\tau = 0$. In the exit channel the effective potential is 9.8 kJ · mol^{-1} higher in the 3D case due to the zero-point energy of the tilt vibration of the CH_3 fragment. This makes the barrier a little bit wider on the exit side, which has a large effect on the dissociation probability, because of the tunneling. Note that when we would treat the reaction coordinate classically that there would be no difference for the two effective potentials, because the heights of both is the same. For a fully classical 2D and 3D simulation there would be a difference in the dissociation probabiliy for translational energies above the minimum barrier height, because the distribution of barrier heights is different. As the zero-point energy of the CH_3 tilt is not large, yet has a large effect on the dissociation probability, the inclusion of other degrees of freedom may have a substantial effect too.

Fig. 2 also shows some results for dissociation with a singly excited CH_3–H stretch. As is to be expected for a late barrier, the dissociation increases enormously. This too can be explained using 1D effective potentials (see Fig. 4). The effective barrier height decreases rapidly with increasing vibrational excitation level, and vanishes already at $v_s = 3$. The effective barrier height is 79.4 kJ · mol^{-1} for $v_s = 0$ and 60.0 kJ · mol^{-1} for $v_s = 1$. This is very similar to what has been found for H_2 model studies [38]. The additional vibrational energy of 33.3 kJ · mol^{-1} is very efficient in inducing dissociation; we can see in Fig. 2 that the dissociation probability curve of $v_s = 1$ is about 22 to 26 kJ · mol^{-1} lower in energy than the one of $v_s = 0$.

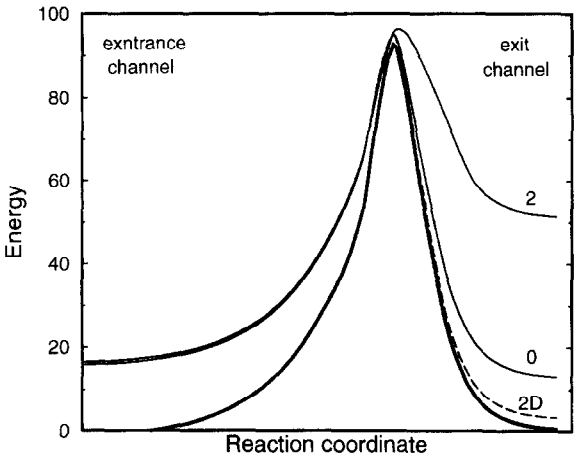

Fig. 3. Effective 1D potentials (in kJ · mol^{-1}) showing the effect of including the rotational degree of freedom. The fat line is the value of the potential-energy surface along the reaction path. The dashed line is the effective potential for the 2D simulation with CH_4 in the ground state. The solid lines are effective potentials for CH_4 in the ground state and in a state excited in τ. The number on the right indicates v_τ ($v_\tau = 0$ correlates with $m_\tau = 0$, and $v_\tau = 2$ with $m_\tau = 1$, because of symmetry). Only potentials for states even in τ are shown.

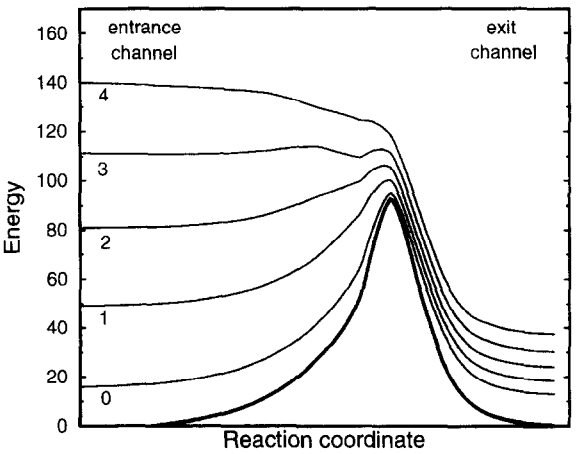

Fig. 4. Effective 1D potentials (in kJ · mol^{-1}) showing the effect of excitation of the CH_3–H stretch. The fat line is the value of the potential-energy surface along the reaction path. The solid lines are effective potentials for CH_4 in the ground state and in states excited initially in s. (They become excited in Z to the right of the barrier.) The numbers on the left indicate v_s.

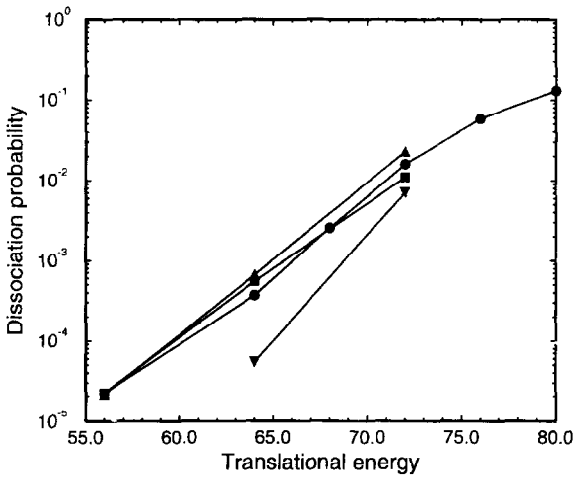

Fig. 5. Dissociation probability as a function of translational energy (in $kJ \cdot mol^{-1}$) for CH_4 initially in the ground state (circles), and rotationally excited states $m_\tau = 1$ (triangles pointing upwards), $m_\tau = -1$ (triangles pointing downwards), and $m_\tau = 2$ (squares). The symbols are simulation results, and the solid lines are guides for the eye.

Fig. 5 shows the dissociation probability for rotational excitation. We see that the initial states even in τ have about the same dissociation probability, but that the one odd in τ has a much lower one. This indicates that the even-τ states do not follow an effective 1D potential. For if they did we would find that the $m_\tau = 1$ initial state would become $v_\tau = 2$ in the exit channel, and $m_\tau = 2$ would become $v_\tau = 4$. The barriers for these processes are much wider than for the lowest effective potential (see Fig. 3), and a drastically reduced dissociation probability would be found. Instead we see that terms that couple the effective potentials are important [38]. Indeed, we hardly find any vibrational excitations of the CH_3 tilt. For the initial state $m_\tau = -1$ the effective potential leads to $v_\tau = 1$. In this case no coupling exists with the lowest effective potential, because it is symmetry forbidden. Consequently, a wider barrier is felt, and the dissociation probability becomes much lower.

That there are substantial coupling terms between the effective potentials can also be seen from the excitations of the CH_3 tilt. Only at the highest translational energy that we looked at ($80\ kJ \cdot mol^{-1}$) did we find an occupation of the $v_\tau = 2$ level in the exit channel comparable to the $v_\tau = 0$ (0.084 and 0.047 being the fractions of the total wavefunction at the end of the simulation ending up in $v_\tau = 0$ and $v_\tau = 2$, respectively). Below $72\ kJ \cdot mol^{-1}$ vibrational excitation of the CH_3 tilt accounts for less than 1% of the wavefunction in the exit channel. On the other hand, as is to be expected for a late barrier, the vibration perpendicular to the surface of the dissociated CH_4 as a whole is highly excited. The effect is stronger than for H_2 as the frequency is lower due to the higher mass of CH_4 [38]. For low translational energies the occupation of the levels scales exponentially with translational energy, as does the dissociation probability. The levels $v_Z = 0$, $v_Z = 1$ and $v_Z = 2$ have also about the same exponential factor as the dissociation probability.

Fig. 6 shows scattering probabilities. The excitation $v_s = 1$ of the CH_3–H stretch seems to scale exponentially, and resembles rather closely the curve of the total dissociation probability. This is, we think, related to the fact that for the reaction path coming from the entrance channel the CH_3–H stretch coordinate stays around its gas phase value for a long time, and only just before the top of the barrier the CH_3–H bond stretches. Consequently, at low translational energies almost all CH_4 is scattered from the surface without really feeling

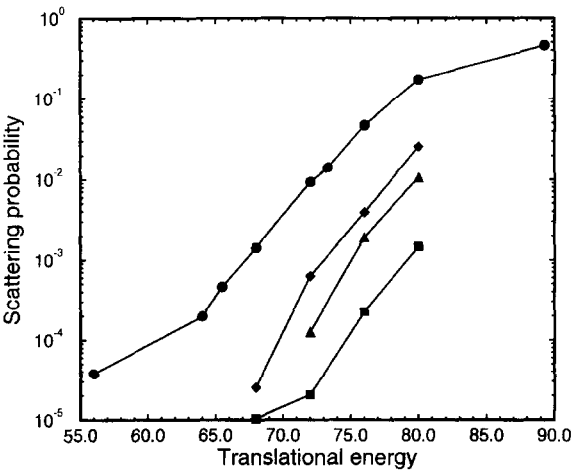

Fig. 6. Scattering probabilities as a function of translational energy (in $kJ \cdot mol^{-1}$) for vibrational and rotation excited levels. Circles indicate excitation to $v_s = 1$, squares to $v_s = 2$, diamonds to $m_\tau = 1$, and triangles to $m_\tau = 2$. The symbols are simulation results, and the solid lines are guides for the eye.

the bend in the reaction path (see Fig. 1). Although the excitation energy of the CH_4 rotation is even much smaller than for the CH_3–H stretch, the rotation is even less excited. The reason for this is that the PES becomes only τ-dependent at the exit side of the barrier. However, once the rotation is excited it is not restricted to just small $|m_\tau|$ values. At $E_T = 80\ kJ \cdot mol^{-1}$ we have found scattering probabilities of 0.83, 0.025, 0.011, 3.8×10^{-3} and 1.0×10^{-3} for $m_\tau = 0$, 1, 2, 3 and 4, respectively.

The 2D simulations show about the same vibrational excitation in the scattered part of the wavefunction as the 3D simulations. More interesting are the scattering results for excited initial states. The scattering of a CH_4 molecule with a singly excited CH_3–H stretch vibration is predominantly adiabatic as long as the dissociation probability is smaller than about 0.1. For energies with a higher dissociation probability there is a strong de-excitation in the scattered part. At $E_T = 56\ kJ \cdot mol^{-1}$ a fraction of 0.573 of the total wavefunction is scattered and a fraction of 0.456 is scattered into $v_s = 0$. Also $v_s = 1$ (0.059) and $v_s = 2$ (0.047) have some population, but other vibrational levels are hardly populated. At this energy there is also substantial excitation of the CH_4 rotation; 0.170 for $m_\tau = 1$ and 0.095 for $m_\tau = 2$. Apart from a shift in the translational energy equal to a vibrational quantum, due to microreversibility the de-excitation probability $v_s = 1 \rightarrow 0$ is equal to the excitation probability $v_s = 0 \rightarrow 1$ [41]. We have used this to increase the number of data points in Fig. 6. If the initial state is rotationally excited then the scattering is adiabatic for the range of translational energies we have looked at.

We would finally like to make a few remarks on the correlation between the excitations. There is a strong correlation in the scattered part of the wavefunction between the rotational and the vibrational excitation. In the rotationally excited levels the vibration is excited more than in the rotational ground state. The reason for this is obviously that the rotational excitation originates from parts of the wavefunction that have extended even beyond the top of the barrier, which leads also to vibrational excitation. As the translational energy becomes higher the correlation becomes stronger, and also more vibrationally excited states become populated. A reverse effect is seen for the rotational ground state. For this state the vibrational ground state is slightly preferred.

There is much less correlation in the dissociated part of the wavefunction. The only clear effect is that the ground state of the CH_3 tilt vibration is a little bit more excited in the vibration perpendicular to the surface than is to be expected based on the population of the perpendicular vibration for the whole dissociated part.

4. Conclusions

We have done quantum simulations for a 3D model of CH_4 dissociation on Ni(111) using the MCTDH method. The PES was developed based on information of DFT calculations. It has a very late barrier and a height of $93.2\ kJ \cdot mol^{-1}$.

The dissociation probability scales exponentially with the translational energy of the methane molecule. From the total energy and the height of the barrier it could be deduced that the discussion occurs via tunneling. The inclusion of the rotation in the simulation of CH_4 decreases the dissociation probability. This is due to the fixed orientation of the CH_3 on the surface, which makes the barrier for the dissociation effectively wider. Because of the late barrier a CH_4 molecule with an excited CH_3–H stretch vibration dissociates much easier. There is a strong tendency to de-excite a rotationally excited CH_4, which has as a consequence that there is only a small effect on the dissociation probability. Only when for symmetry reasons this de-excitation is not allowed, the CH_3 tilt will be excited, which reduces the dissociation probability.

Excitation of the CH_3–H in scattered CH_4 resembles the dissociation probability as both require enough translational energy so that the wavefunction can sample the region of the PES around the top of the barrier, where the C–H bond is stretched. The rotation of scattered CH_4 is only excited at the highest translational energy we looked at ($80\ kJ \cdot mol^{-1}$), even though the excitation energy is very low. This is because the PES has no rotational dependence on the entrance side of the barrier. When the rotation does become excited the excited rotational levels are also more

vibrationally excited than the rotational ground state.

Acknowledgements

A.P.J.J. would like to thank Cray Research Inc. and NCF (Stichting Nationale Computer Faciliteiten) for financial support through a Cray Research Grant. H.B. would like to thank SON (Stichting Scheikundig Onderzoek in Nederland) and NWO (Nederlandse Organisatie voor Wetenschappelijk Onderzoek) for their financial support.

References

[1] J.P. Van Hook, Catal. Rev. Sci. Eng. 21 (1980) 1.
[2] C.T. Rettner, H.E. Pfnür and D.J. Auerbach, Phys. Rev. Lett. 54 (1985) 2716.
[3] C.T. Rettner, H.E. Pfnür and D.J. Auerbach, J. Chem. Phys. 84 (1986) 4163.
[4] M.B. Lee, Q.Y. Yang, S.L. Tang and S.T. Ceyer, J. Chem. Phys. 85 (1986) 1693.
[5] M.B. Lee, Q.Y. Yang and S.T. Ceyer, J. Chem. Phys. 87 (1987) 2724.
[6] A.C. Luntz and D.S. Bethune, J. Chem. Phys. 90 (1989) 1274.
[7] G.R. Schoofs, C.R. Arumanayagam, M.C. McMaster and R.J. Madix, Surf. Sci. 215 (1989) 1.
[8] A.V. Hamza and R.J. Madix, Surf. Sci. 179 (1987) 25.
[9] C.T. Rettner, H.A. Michelsen and D.J. Auerbach, J. Chem. Phys. 102 (1995) 4625.
[10] H. Burghgraef, A.P.J. Jansen and R.A. van Santen, J. Chem. Phys. 98 (1993) 8810.
[11] H. Burghgraef, A.P.J. Jansen and R.A. van Santen, Chem. Phys. 177 (1993) 407.
[12] H. Burghgraef, A.P.J. Jansen and R.A. van Santen, Faraday Discuss. Chem. Soc. 96 (1993) 337.
[13] H. Burghgraef, A.P.J. Jansen and R.A. van Santen, J. Chem. Phys. 101 (1994) 11012.
[14] H. Burghgraef, A.P.J. Jansen and R.A. van Santen, Surf. Sci. 324 (1995) 345.
[15] U. Manthe, H.-D. Meyer and L.S. Cederbaum, J. Chem. Phys. 97 (1992) 3199.
[16] A.P.J. Jansen, J. Chem. Phys. 99 (1993) 4055.
[17] U. Manthe, H.-D. Meyer and L.S. Cederbaum, J. Chem. Phys. 97 (1992) 9062.
[18] U. Manthe and A.D. Hammerich, Chem. Phys. Lett. 211 (1993) 7.
[19] A.D. Hammerich, U. Manthe, R. Kosloff, H.-D. Meyer and L.S. Cederbaum, J. Chem. Phys. 101 (1994) 5623.
[20] L. Liu, J.-Y. Fang and H. Guo, J. Chem. Phys. 102 (1995) 2404.
[21] J.-Y. Fang and H. Guo, J. Chem. Phys. 102 (1995) 1944.
[22] A. Jäckle and H.-D. Meyer, submitted to J. Chem. Phys.
[23] J.-Y. Fang and H. Guo, J. Chem. Phys. 101 (1994) 5831.
[24] J.-Y. Fang and H. Guo, Chem. Phys. Lett. 235 (1995) 341.
[25] A. Capellini, A.P.J. Jansen, G.-J. Kroes and R.C. Mowrey, in preparation.
[26] A.C. Luntz, private communications.
[27] A.C. Luntz and J. Harris, Surf. Sci. 258 (1991) 397.
[28] A.C. Luntz and J. Harris, J. Vac. Sci. Techn. A 10 (1992) 2292.
[29] A.C. Luntz and J. Harris, J. Chem. Phys. 96 (1992) 7954.
[30] J.H. McCreery and G. Wolken Jr., J. Chem. Phys. 67 (1977) 2551.
[31] U. Manthe, J. Chem. Phys. 101 (1994) 2652.
[32] A.P.J. Jansen, J. Chem. Phys. 101 (1994) 2654.
[33] G. Hall and J.M. Watt, Modern Numerical Methods for Ordinary Differential Equations (Clarendon, Oxford, 1976).
[34] The NAG Fortran Library Manual, Mark 16, Vol. 2 (NAG Ltd., Oxford, 1993) routine D02CBF.
[35] L.I. Schiff, Quantum Mechanics (McGraw-Hill, New York, 1968).
[36] T.P. Beebe, D.W. Goodman, B.D. Kay and J.T. Yates Jr., J. Chem. Phys. 87 (1987) 2305.
[37] M. Karikorpi, S. Holloway, N. Henriksen and J.K. Nørskov, Surf. Sci. 179 (1987) L41.
[38] D. Halstead and S. Holloway, J. Chem. Phys. 93 (1990) 2859.
[39] R.A. Marcus, J. Chem. Phys. 45 (1966) 4493.
[40] P.G. Mezey, Potential Energy Hypersurfaces (Elsevier, Amsterdam, 1987).
[41] G. Darling and S. Holloway, Surf. Sci. 307–309 (1994) 153.